

---

# EvoFed: Leveraging Evolutionary Strategies for Communication-Efficient Federated Learning

---

Mohammad Mahdi Rahimi   Hasnain Irshad Bhatti   Younghyun Park  
Humaira Kousar   Jaekyun Moon

KAIST

{mahi,hasnain,dnffkf369,humairakousar32}@kaist.ac.kr  
jmoon@kaist.edu

## Abstract

Federated Learning (FL) is a decentralized machine learning paradigm that enables collaborative model training across dispersed nodes without having to force individual nodes to share data. However, its broad adoption is hindered by the high communication costs of transmitting a large number of model parameters. This paper presents EvoFed, a novel approach that integrates Evolutionary Strategies (ES) with FL to address these challenges. EvoFed employs a concept of ‘fitness-based information sharing’, deviating significantly from the conventional model-based FL. Rather than exchanging the actual updated model parameters, each node transmits a distance-based similarity measure between the locally updated model and each member of the noise-perturbed model population. Each node, as well as the server, generates an identical population set of perturbed models in a completely synchronized fashion using the same random seeds. With properly chosen noise variance and population size, perturbed models can be combined to closely reflect the actual model updated using the local dataset, allowing the transmitted similarity measures (or fitness values) to carry nearly the complete information about the model parameters. As the population size is typically much smaller than the number of model parameters, the savings in communication load is large. The server aggregates these fitness values and is able to update the global model. This global fitness vector is then disseminated back to the nodes, each of which applies the same update to be synchronized to the global model. Our analysis shows that EvoFed converges, and our experimental results validate that at the cost of increased local processing loads, EvoFed achieves performance comparable to FedAvg while reducing overall communication requirements drastically in various practical settings.

## 1 Introduction

Federated Learning (FL) provides a decentralized machine learning framework that enables model training across many devices, known as clients, without needing to collect and process sensitive client data on the centralized server [1]. The typical FL process begins with each client downloading an identical initialized model from a central server, performing model updates with local data, and then uploading the updated local model for the next communication round. Subsequently, the server combines the uploaded models to refine the global model, typically using a technique like FedAvg [2]. This iterative cycle repeats for a fixed number of rounds, ensuring collaborative model improvement across clients.

Although FL provides notable benefits, such as a certain level of privacy preservation and the utilization of diverse data sources, one of the major challenges associated with FL is the significant

communication overhead involved in transmitting model updates between clients and the server, especially when dealing with models that have a large number of parameters.

Various strategies have been developed to mitigate the communication burden in FL. These techniques can be broadly classified into three categories: i) Compressing updates: sparsification [1], structured updates [3], and quantization [4, 5] reduce the size of transmitted model updates, ii) Local computation: performing multiple local epochs at the clients [6] lessens the frequency of communication with the server, and iii) Advanced aggregation methods and client selection: MOCHA [7] enhances the efficacy of update aggregation and [8, 9] reduce communication by only selecting a subset of clients to participate in each training round.

Existing FL techniques primarily rely on transmitting gradient signals or model updates, which are computed through backpropagation (BP). On the other hand, Evolutionary Strategies (ES) [10–12] update model parameters by utilizing fitness values obtained from evaluating a population of models. This approach eliminates the need for a gradient signal, as depicted in Fig. 1. Recent advances in neuroevolution have shown promise in supervised settings and competitive performance with reinforcement learning in control tasks [13–15, 11, 16–18]. In this context, ES offers a distinct advantage compared to traditional BP methods. This paradigm shift opens up the possibility of searching for novel solutions beyond the gradient-based methods. However, it is critical to note that ES, despite its potential, still lags behind gradient-based methods in certain problems like supervised learning. Fig. 2(a) reveals the performance gap between ES and BP. This emphasizes the need for a balanced approach that would leverage the strengths of both ES and gradient-based methods to achieve optimal results.

Our proposed method operates on the premise of incorporating high-quality gradient signals into the evaluation process of ES. The process can be formalized as follows:

Given a base model, denoted by  $\theta$ , we instantiate a population  $P$  comprised of  $N$  model samples. Each individual sample,  $\theta^i$ , is derived by adding random perturbations to  $\theta$ . Unlike traditional ES, where the fitness of  $\theta^i$  corresponds to its performance on the task, we instead assess the fitness of each sample  $\theta^i$  by measuring its similarity to  $\theta'$ , the model parameters updated through gradient descent steps. This operation effectively exploits the gradient signal to construct a fitness vector, a process we term Population-Based Gradient Encoding (PBGE). Fig. 2(b) shows the results of a representative experimental setting where PBGE is able to follow BP closely on the FMNIST dataset while maintaining an effective compression rate of over 98.8%. In particular, this method significantly outperforms sparsification strategies at equivalent compression rates.

In the context of FL, the gradient signal can be encoded into a fitness vector for the population of models and communicated to the server. For global synchronization, a well-established approach like FedAvg would involve reconstruction and aggregation of the clients' models and sharing of the aggregated model with the clients. However, by utilizing shared random seeds, we can ensure uniformity in the generated populations between clients and the server. This allows us to transmit and aggregate only the small fitness vectors without reconstructing the models, reinforcing communication efficiency. In addition, there is an advantage in implementing extra privacy measures. When encryption is desired, the required overhead would be much smaller with the fitness vectors than with the model parameter vectors because of the size difference. A brief overview of EvoFed is shown in Fig. 3 (the detailed methodology is provided in Section 4).

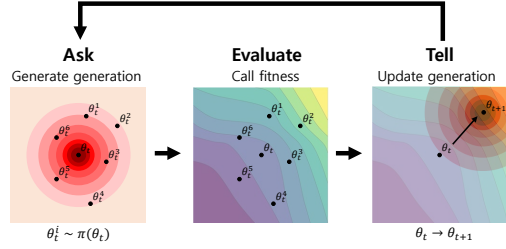
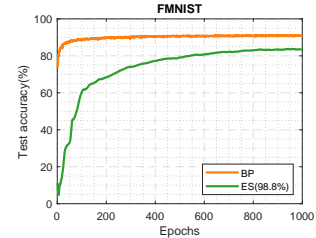
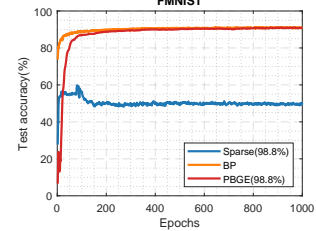


Figure 1: ES follows an iterative ask, evaluate, and tell approach for optimization. The strategy starts by generating candidate solutions of a base model(*ask*), which are then assessed using a fitness measure (*evaluate*). The base model is updated towards a better solution using the evaluation results (*tell*).



(a) Estimation with ES



(b) The proposed method

Figure 2: Test accuracy on FMNIST dataset comparing (a) ES against BP, and (b) PBGE with BP and Sparse with 98.8% compression.

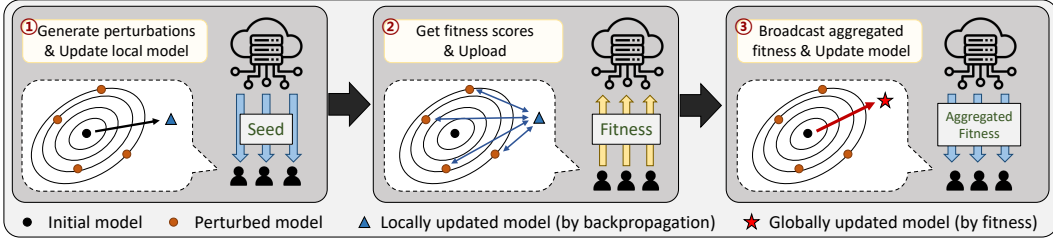


Figure 3: Overview of the proposed EvoFed: (1) Using the shared random seed, each client generates a population of perturbations around the local model. Each client also performs a gradient update of the local model using the local data as in conventional FL. (2) Each client evaluates the fitness of each perturbed model with respect to the updated model. The fitness values are communicated to the server. (3) The server aggregates the fitness values. Clients update their local models using broadcast aggregated fitness.

**Contributions.** To summarize, our main contribution is to introduce a novel concept of Population-Based Gradient Encoding (PBGE), which allows an accurate representation of the large local gradient vector using a relatively small fitness vector, significantly reducing the communication burden as well as the encryption overhead in FL environments. We also propose and verify the EvoFed framework that integrates PBGE into federated learning based on the exchange and aggregation of the fitness vectors between clients and the server.

Our approach achieves similar performance to FedAvg on both FMNIST and CIFAR-10 datasets. The advantage is that our scheme achieves very high compression, exceeding 98.8% on FMNIST and 99.7% on CIFAR-10 in key practical settings. Significantly, our EvoFed model also outperforms traditional compression methods, offering superior results at similar compression rates. The price we pay is the overhead of generating a population of perturbed models and computing similarity measures. This overhead could be substantial in the form of increased local processing time depending on the size of the population, but the client computational load can be traded with local memory space by employing parallel processing. In addition, as discussed later, reduce population size without affecting performance.

## 2 Related Work

**Federated Learning.** Several techniques have been proposed to alleviate the communication overhead in FL, such as model compression [1, 19, 20], distillation techniques [21–25], and client update subsampling [26, 27]. However, these approaches often come with trade-offs, including increased convergence time, lower accuracy, or additional computational requirements. More importantly, they still require the exchange of model parameters, which requires substantial communication bandwidth. Furthermore, [28] shows that the gradient sparsity of all participants has a negative impact on global convergence and communication complexity in FL.

**Evolutionary Strategies.** ES are black-box optimization algorithms inspired by biological evolution [29]. ES algorithms iteratively refine a population of solutions based on fitness evaluations. Natural Evolution Strategies (NES) is a specific variant of ES [30, 12, 31–35]. Within the NES framework, the distribution  $p_\psi(\theta)$ , parameterized by  $\psi$ , is adopted to represent the population and maximize the average objective value  $\mathbb{E}_{\theta \sim p_\psi}[f(\theta)]$  via stochastic gradient ascent, where  $f(\theta)$  is the fitness function. NES algorithms leverage a score function estimator as in [10]. Our method follows the guidelines provided by [36], where the parameter distribution  $p_\psi$  is a factored Gaussian. Accordingly, we can represent  $\mathbb{E}_{\theta \sim p_\psi}[f(\theta)]$  using the mean parameter vector  $\theta$ , such that  $\mathbb{E}_{\theta \sim p_\psi}[f(\theta)] = \mathbb{E}_{\epsilon \sim \mathcal{N}(0, I)}[f(\theta + \sigma\epsilon)]$ . Given a differentiable function estimator, the well-known conversion procedure allows optimization over  $\theta$  to be rewritten as (see, for example, [37, 11, 38])

$$\nabla_{\theta} \mathbb{E}_{\epsilon \sim \mathcal{N}(0, I)}[f(\theta + \sigma\epsilon)] = \frac{1}{\sigma} \mathbb{E}_{\epsilon \sim \mathcal{N}(0, I)}\{f(\theta + \sigma\epsilon)\epsilon\}. \quad (1)$$

The strategy of sharing seeds for random number generators to synchronize parallel processes and maintain consistency is a well-established practice in areas ranging from parallel simulations to cryptographic protocols [39]. The appeal of shared random seeds stems from their ability to offer deterministic randomness, ensuring that multiple entities, operating independently, can produce synchronized and identical random outputs. Within the realm of ES, this concept was effectively harnessed by [36] to address the challenge of scalability. We also utilize the shared random seeds to

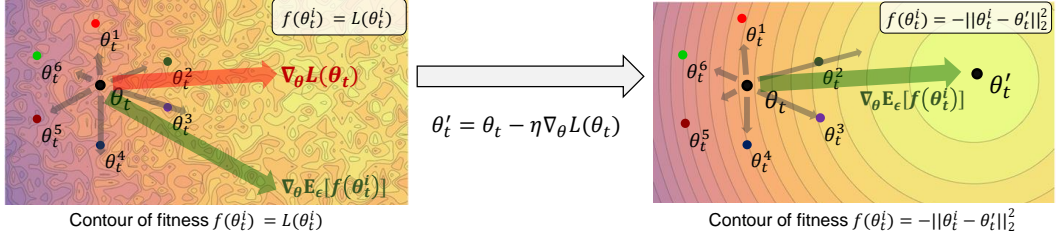


Figure 4: Illustration of one update step of typical ES and the proposed Population-Based Gradient Encoding (PBGE) strategy. **Left:** using loss value  $L(\theta)$  directly for the fitness  $f(\theta)$ , as in existing ES, leads to an inherently noisy estimate of the gradient signal  $\nabla_{\theta} \mathbb{E}_{\epsilon}[f(\theta + \sigma\epsilon)]$  due to the noisy loss surface. **Right:** PBGE defines fitness as the distance to the updated model  $\theta'$  obtained through BP (i.e.,  $f(\theta) = -\|\theta - \theta'\|_2^2$ ). This enables the reliable estimate of  $\theta'$  on the convex surface. By sampling a sufficient number of perturbations  $\epsilon_i$ , a decent gradient signal can be obtained, which aligns to the true gradient signal  $\nabla_{\theta} L(\theta)$  computed from the BP.

scale down the communication load in a distributed setting. However, the key difference is that the work of [36] distributes the perturbations into multiple workers dealing with a single global objective, whereas our method generates identical perturbations across all clients, with each having a distinct objective. An important consequence is that with our method, each client only needs to communicate  $N$  fitness values to update the model, instead of  $MN$  values in [36] with  $M$  denoting the number of nodes, enabling scalability regardless of the number of clients.

**Federated Learning and Evolutionary Strategies.** Several studies have explored the optimization of FL using ES. For instance, [40] introduced an evolutionary approach for network architecture search (NAS) in real-time FL, which minimizes local payload while optimizing model performance. Sparse evolutionary training (SET) [41] substitutes fully connected layers in neural networks with sparse layers to decrease the number of model parameters. Furthermore, [42] presented the SET algorithm that optimizes neural networks in FL via a bi-objective method to maximize accuracy performance while minimizing communication overhead. Additionally, [43] introduces the MOEA/D framework [44] to the environment of FL and FLEA [45] utilized Evolutionary Algorithms in FL setup at the client-level to evolve models.

While these studies have made significant contributions, the present work establishes a unique way of using ES as a method to reduce communication overhead in FL by transmitting fitness values instead of model parameters. In particular, the new gradient-driven fitness function essentially separates our work from the traditional utilization of ES for compression.

### 3 Population-Based Gradient Encoding

This work focuses on the process of encoding gradient information through an identical population of models generated at both ends of some network link. Population distribution is a zero mean isotropic multivariate Gaussian with fixed covariance  $\sigma^2 I$ . We also adopt ‘mirrored sampling’ [46, 47] for variance reduction where the Gaussian noise vector  $\epsilon$  is instantiated with pairs of perturbations  $\epsilon, -\epsilon$ .

Given the reference point  $\theta' = \theta - \eta \nabla L(\theta)$  where  $\eta$  is the learning rate in the BP-based gradient update and  $\nabla L(\theta)$  represents the gradient derived from the data, we define the fitness function  $f(\theta)$  to measure the similarity between the model parameters  $\theta$  and  $\theta'$ :  $f(\theta) = -\|\theta - \theta'\|_2^2$ . This choice ensures that the gradient of the expectation,  $\nabla_{\theta} \mathbb{E}_{\epsilon \sim \mathcal{N}(0, I)}[f(\theta + \sigma\epsilon)]$ , aligns with the actual gradient  $\nabla L(\theta)$ , effectively encoding the gradient information in the fitness values:

$$\nabla_{\theta} \mathbb{E}_{\epsilon \sim \mathcal{N}(0, I)}[-\|(\theta + \sigma\epsilon) - \theta'\|_2^2] = -\nabla_{\theta} \|\theta - \theta'\|_2^2 = 2(\theta - \theta') \quad (2)$$

where the first equality simply follows from the assumption that  $\epsilon$  is zero-mean. The visual representation of this process is illustrated in Fig. 4. Eq. 2 gives  $\theta' = \theta - \frac{1}{2} \nabla_{\theta} \mathbb{E}_{\epsilon}[-\|(\theta + \sigma\epsilon) - \theta'\|_2^2]$ , and comparing with the BP operation  $\theta' = \theta - \eta \nabla L(\theta)$ , we have

$$\eta \nabla_{\theta} L(\theta) = \frac{1}{2} \nabla_{\theta} \mathbb{E}_{\epsilon \sim \mathcal{N}(0, I)}[-\|(\theta + \sigma\epsilon) - \theta'\|_2^2].$$

Now also utilizing Eq. 1, we write

$$\eta \nabla_{\theta} L(\theta) = \frac{1}{2\sigma} \mathbb{E}_{\epsilon \sim \mathcal{N}(0, I)}\{f(\theta + \sigma\epsilon)\epsilon\} \quad (3)$$

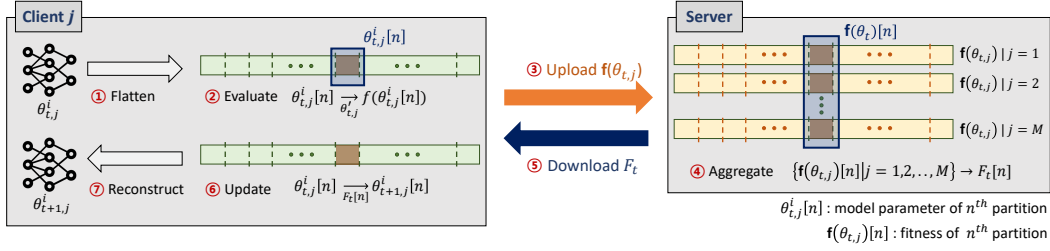


Figure 5: Partition-based Model Parameter Compression. Illustration of dividing model parameters  $\theta$  into  $K$  partitions and compressing them individually using PBGE.

where  $f$  is the specific distance-based fitness function defined above. Approximating the expectation by sampling, we further write

$$\eta \nabla_{\theta} L(\theta) \approx \frac{1}{2N\sigma} \sum_{i=1}^N f(\theta + \sigma \epsilon_i) \epsilon_i \quad (4)$$

which shows how the gradient update information can be encoded using the fitness values  $f(\theta + \sigma \epsilon_i)$  corresponding to the perturbations  $\epsilon_i$ . Consequently, this removes the need to evaluate each perturbation with the dataset, as is done in existing ES, and the entire update process is encoded with low-cost distance measurement.

Finally, the update on  $\theta$  itself based on the fitness values is naturally given by

$$\theta' \approx \theta + \frac{1}{2N\sigma} \sum_{i=1}^N f(\theta + \sigma \epsilon_i) \epsilon_i \quad (5)$$

allowing a remote model update based on the transmitted  $f(\theta + \sigma \epsilon_i)$  values with the shared knowledge of the  $\epsilon_i$  values.

The implemented algorithm consistently executes three steps: (i) Compute the target  $\theta'$  through gradient descent, (ii) Implement perturbations to the model parameters and assess the perturbed parameters by computing their Euclidean distance to  $\theta'$ , and (iii) Utilize the assessment results and encode the gradient with the fitness measures.

**Partitioning.** In the context of PBGE, the fitness function indicates the model distance, not the model performance on client data. This feature enables a unique partition-based approach for handling a large number of model parameters. Here, the parameters, flattened into a vector  $\theta$ , are split into  $K$  partitions:  $\theta[1], \theta[2], \dots, \theta[K]$ . Each partition is then effectively encoded individually using PBGE, which is advantageous when working with large models, as storing a large population of those may be burdensome for clients with limited memory. Partitioning allows us to compute  $K$  fitness values per each perturbation, providing  $K$  times more reference points to encode the gradient information given a population size. Hence, even with a small population size (requiring less memory), we achieve robust performance as validated by the empirical results provided in Supplementary Materials. Essentially, partitioning provides a tradeoff of memory with communication as more fitness values now need to be communicated per each perturbation. This partitioning process is visualized in Fig. 5. Notably, this partitioning technique can be used with any model architecture, regardless of its specific design, providing a practical and efficient means of compressing large models.

## 4 EvoFed

EvoFed operates on the principle that the evolutionary update step depends only on the fitness values given the perturbation samples. In the FL context, we can leverage this characteristic to devise an accurate yet communication-efficient strategy for model updates. This section provides a detailed exposition of our methodology, breaking it down into stages for clarity. This iterative process, as outlined in Algorithm 1, aims to gradually converge the model parameters at all nodes to an optimal solution while minimizing data transmission during each update. An overall view of our proposed methodology is depicted in Fig. 3.

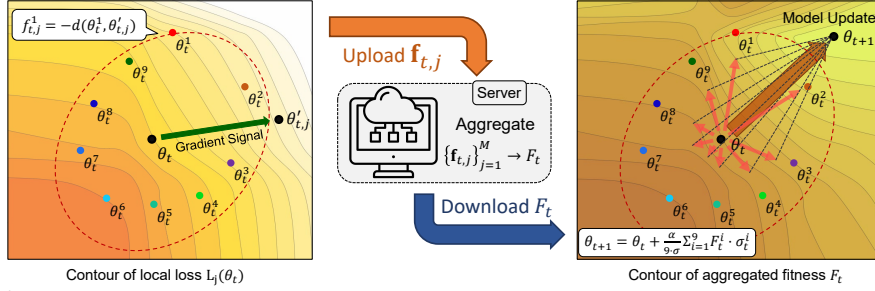


Figure 6: Local Updates and Fitness Evaluation (left) and Server/Client-side Update (right). Left: Client performs BP on local data  $\theta_t$  to obtain  $\theta_{t,j}^i$ , evaluates fitness  $f_{t,j}^i$  by distance measure (e.g. L2) with  $\theta_t^i$ , and uploads  $\mathbf{f}_{t,j}$  to the server. Right: After obtaining the aggregated fitness  $\mathbf{F}_t$ , all nodes update the baseline model  $\theta_t$  according to Eq. 9.

#### 4.1 Initial Setup

The initialization of the server and clients in EvoFed begins with the same baseline model, denoted by  $\theta_0$ . A key assumption is that the server and all clients share the same seed (e.g., via broadcasting) for identical random population generation. This approach ensures consistent baseline models and populations across all nodes.

In this step, a population of candidate solutions (in this case, models) is generated by adding random perturbations to the current best solution (the baseline model). The generation of an  $i$ -th member of the model population can be formulated as follows:

$$\theta_t^i = \theta_t + \mathcal{N}(0, \sigma I) \quad (6)$$

Here,  $\mathcal{N}(0, \sigma I)$  represents the perturbations sampled from a multivariate normal distribution with zero mean and a shared covariance matrix  $\sigma I$ . We also denote the population at each node at any given time  $t$  as  $\mathbf{P}_t = \{\theta_t^1, \theta_t^2, \dots, \theta_t^N\}$ , where  $\theta_t^i$  represents the  $i$ -th model in the population generated by adding the  $i$ -th perturbation to the baseline model parameters, and  $N$  is the size of the population.

#### 4.2 Local Updates and Fitness Evaluation

Each client node begins by executing BP on its local dataset, using the baseline model,  $\theta_t$ , resulting in an updated model,  $\theta_t'$ . Following this, the fitness of each member  $\theta_t^i$  in the local population,  $\mathbf{P}_t$ , is evaluated. This evaluation is done by measuring the similarity between  $\theta_t'$  and  $\theta_t^i$ . The L2 norm or Euclidean distance serves as the measure of this similarity. The fitness of  $\theta_t^i$  is represented as  $f(\theta_t^i)$ :

$$f(\theta_t^i) = -\|\theta_t' - \theta_t^i\|_2^2 \quad (7)$$

The process of local update and fitness evaluation is illustrated in Fig. 6. The fitness values are the only information that needs to be communicated among nodes. The fitness vectors are significantly smaller in size compared to the model parameter vectors, which helps reduce the communication overhead. Hence, each client sends a fitness vector,  $\mathbf{f}_t = \{f(\theta_t^1), f(\theta_t^2), \dots, f(\theta_t^N)\}$  corresponding to all population members, to the server.

#### 4.3 Server-side Aggregation and Update

The server's responsibility is to aggregate the fitness values reported by all client nodes, forming a global fitness vector  $\mathbf{F}_t$  comprising  $N$  elements, with  $\mathbf{F}_t^i$  representing the fitness value of the  $i^{\text{th}}$  member of the population. Each client's contribution to  $\mathbf{F}_t$  is weighted by their respective batch size  $b_j$ , giving a larger influence to clients with potentially more accurate local updates.

The global fitness vector  $\mathbf{F}_t$  is computed as follows:

$$\mathbf{F}_t = \frac{1}{\sum_{j=1}^M b_j} \sum_{j=1}^M b_j \mathbf{f}_{t,j} \quad (8)$$

where  $M$  is the total number of clients and  $\mathbf{f}_{t,j}$  is the fitness value from client  $j$  at time  $t$ . After the aggregation, the server broadcasts  $\mathbf{F}_t$  so that each client updates the baseline model  $\theta_t$ .



---

**Algorithm 1** EvoFed: Federated Learning with Evolutionary Strategies
 

---

```

1: Input: Learning rates  $\eta, \alpha$ , population size  $N$ , noise std  $\sigma$ , seed  $s$ 
2: Initialize: server and  $M$  clients with seed  $s$  and identical parameters  $\theta_0$  and  $\theta_{0,j}$  respectively
3: for each communication round  $t = 0, 1, \dots, T - 1$  in parallel do
4:   for each client  $j$  in parallel do
5:      $\theta'_{t,j} = \theta_{t,j} - \eta \nabla_{\theta} L(\theta'_{t,j})$  //Backpropagation Update
6:     Sample  $\epsilon_t^i \sim \mathcal{N}(0, \sigma I)$  //Sample perturbations
7:      $\theta_{t,j}^i = \theta_{t,j} + \epsilon_t^i$  for  $i = 1, \dots, N$  //Initialize population
8:      $\mathbf{f}_{t,j}^i = -\|\theta_{t,j}^i - \theta'_{t,j}\|_2^2$  for  $i = 1, \dots, N$  // Compute fitness vector using  $L_2$  calculation
9:      $\mathbf{F}_t^i = \frac{1}{\sum_j b_j} \sum_j b_j \mathbf{f}_{t,j}^i$  for  $i = 1, \dots, N$  // Server averages fitness vectors
10:     $\theta_{t+1} = \theta_t + \frac{\alpha}{N\sigma} \sum_{i=1}^N \mathbf{F}_t^i \cdot \epsilon_t^i$  // Server updates model using the aggregated fitness
11:    Broadcast  $\{\mathbf{F}_t^1, \mathbf{F}_t^2, \dots, \mathbf{F}_t^N\}$ 
12:    for each client  $j$  in parallel do
13:       $\theta_{t+1,j} = \theta_{t,j} + \frac{\alpha}{N\sigma} \sum_{i=1}^N \mathbf{F}_t^i \cdot \epsilon_t^i$  // Client updates model using the aggregated fitness
  
```

---

#### 4.4 Broadcasting Fitness

Once the aggregation is complete, the server broadcasts  $\mathbf{F}_t$  to all client nodes, maintaining synchronicity across the network. This only involves the transmission of the fitness vector, again reducing communication overhead. The aggregated fitness vector can be used by the local clients (as well as by the server, if needed) to update the local models.

#### 4.5 Client-side Update

When the global fitness vector  $\mathbf{F}_t$  is received from the server, the clients can update their local model following Eq. 5. This strategy involves the addition of a weighted sum of noise vectors to the current model parameters, where the weights are aggregated fitness values:

$$\theta_{t+1} = \theta_t + \frac{\alpha}{N\sigma} \sum_{i=1}^N \mathbf{F}_t^i \cdot \epsilon_t^i \quad (9)$$

where  $\epsilon_t^i$  is the  $i$ -th noise vector from the population at time  $t$ .

Notably, the right side of Eq. 9 can be shown equivalent to the average of all locally updated models akin to FedAvg, i.e., it is straightforward to show that

$$\theta_{t+1} = \frac{1}{\sum_j b_j} \sum_{j=1}^M b_j \theta_{t+1,j} \quad (10)$$

where  $\theta_{t+1,j}$  is the updated model of client  $j$  at time  $t + 1$  defined as

$$\theta_{t+1,j} = \theta_t + \frac{\alpha}{N\sigma} \sum_{i=1}^N f_{t,j}^i \cdot \epsilon_t^i. \quad (11)$$

#### 4.6 Convergence Analysis

**Theorem 1.** Suppose that  $L_j(\theta)$  is the  $\beta$ -smooth function, i.e.,  $\|\nabla L_j(u) - \nabla L_j(v)\| \leq \beta \|u - v\|$  for any  $u, v$ , and also suppose that the variance of the stochastic gradient of  $D_j$  is bounded, i.e.,  $\mathbb{E}\|\nabla L_j(\theta) - \tilde{\nabla} L_j(\theta)\|^2 \leq B^2$  for all  $j$ . When perturbation  $\epsilon^i$  is sampled, a conditioned mirrored sampling is applied such that  $\frac{1}{N} \sum_{i=1}^N \epsilon^i = 0$ ,  $\frac{1}{N} \sum_{i=1}^N (\epsilon^i)^2 \leq G^2$ ,  $\frac{1}{N} \sum_{i=1}^N (\epsilon^i)^3 = 0$ . Given a decreasing learning rate  $\eta_t < \frac{1}{4\alpha\beta}$ , EvoFed converges in the sense of

$$\frac{1}{H_T} \sum_{t=0}^{T-1} \eta_t \mathbb{E} \left[ \|\nabla L(\theta_t)\|^2 \right] \leq \frac{\mathbb{E}[L(\theta_0)] - L^*}{\alpha G^2 H_T} + 4\alpha\beta B^2 \left( \frac{1}{H_T} \sum_{t=0}^{T-1} \eta_t^2 \right)$$

where  $H_T = \sum_{t=0}^{T-1} \eta_t$ , and  $L^*$  represents the minimum value of  $L(\theta)$ .

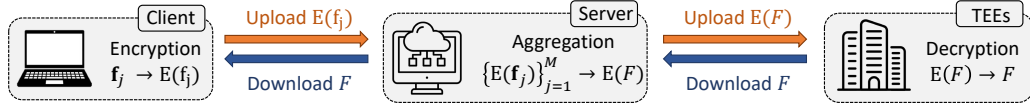


Figure 7: Privacy enhancement through Fully Homomorphic Encryption and Trusted Execution Environments.

Given a decreasing learning rate (e.g.,  $\eta_t = \frac{\eta_0}{1+t}$ ), it can be seen that  $H_T = \sum_{t=0}^{T-1} \eta_t \rightarrow \infty$  as  $T$  increases, while  $\sum_{t=0}^{T-1} \eta_t^2 < \infty$ . Consequently, the upper bound stated in Theorem 1 approaches 0 as  $T$  grows, ensuring convergence towards a stationary point. The detailed discussions and the proof can be found in Supplementary Materials.

#### 4.7 EvoFed and Privacy Enhancements

Unlike other FL methods, EvoFed operates on fitness measures. Encryption on smaller fitness vectors requires a lower overhead compared to encryption on large model parameter vectors. Fig. 7 shows Fully Homomorphic Encryption (FHE) [48–50] that allows aggregation of encrypted data on the server while keeping individual client data confidential. For the decryption of the aggregated fitness vector, EvoFed can leverage third-party Trusted Execution Environments (TEEs), such as Intel SGX [51], providing a secure space for sensitive computations.

#### 4.8 Partial Client Participation

When FL has to operate with a large client pool, a typical practice is to select only a subset of clients in each global round. In EvoFed, this means that the newly joined clients in a given round can either download the latest model or else the last  $k$  fitness vectors from the server, where  $k$  is the time gap from the last participation. In the latter case, the model updates from Eq. (9) can be modified to accommodate  $k$ -step updates:

$$\theta_t = \theta_{t-k} + \frac{\alpha}{N\sigma} \sum_{l=1}^k \sum_{i=1}^N \mathbf{F}_{t-l}^i \cdot \epsilon_{t-l}^i. \quad (12)$$

Note that even in the former case where the latest model is downloaded by the newly joined clients, the level of security is not compromised as far as the client-to-server messages are concerned.

## 5 Experiments

Our algorithm’s effectiveness is assessed on three image classification datasets: FMNIST [52], MNIST [53], and CIFAR-10 [54]. Both MNIST and FMNIST contain 60,000 training samples and 10,000 test samples, whereas CIFAR-10 is composed of 50,000 training samples and 10,000 test samples. We employ a CNN model having 11k parameters for the MNIST and FMNIST datasets and a more substantial model with 2.3M parameters for CIFAR-10. A grid search has been conducted to identify the optimal performance hyperparameters for each baseline, as outlined in the results section. We take into account both global accuracy and communication costs to ascertain hyperparameters that maximize accuracy while minimizing communication overhead.

**Data Distribution.** We distribute the training set of each dataset among clients for model training, and the performance of the final global model is evaluated using the original test set. Our experimental setup contains  $M = 5$  clients with non-IID data distribution (assigning two classes to each client).

**Implementation Details.** Our EvoFed framework is built using JAX [55], which facilitates extensive parallelization and, in particular, consistent random number generation across a large number of nodes. We have implemented our framework on the Evosax [56] library, a convenient tool for the ES algorithm. EvoFed is configured with a population size of 128 and a mini-batch size of 256 for MNIST / FMNIST and 64 for CIFAR-10. We perform ten local epochs (performing ten BP steps before fitness calculation) and train over 1,000 global rounds.

**Baselines.** We compare the performance of the proposed EvoFed with BP, FedAvg, ES, FedAvg with quantization (Fed-quant), and FedAvg with Sparsification (Fed-sparse). In each scenario, we push for maximum compression, stopping right before the model starts to show performance degradation relative to FedAvg with no compression. BP provides the upper-performance baseline, while ES serves as a reference emphasizing the significance of PBGE.



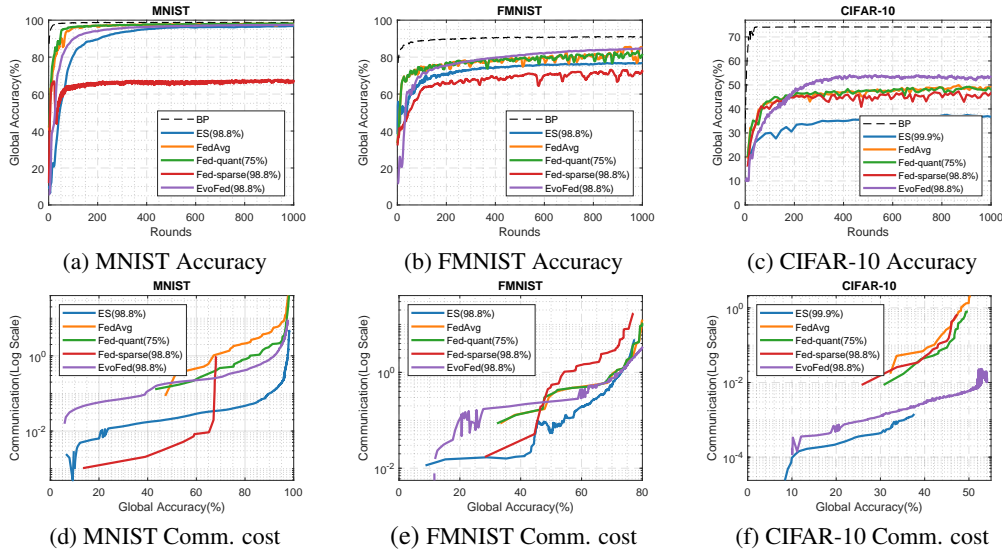


Figure 8: Performance comparison of EvoFed and baseline methods on MNIST, FMNIST, and CIFAR-10 datasets. The top row displays the accuracy achieved by each method on the respective datasets, while the bottom row illustrates the communication cost associated with each method.

Methods	MNIST			FMNIST			CIFAR-10		
	Comm. Cost (MB)		Max Acc.	Comm. Cost (MB)		Max Acc.	Comm. Cost (GB)		Max Acc.
	90% Acc.	Max Acc.		70% Acc.	Max Acc.		45% Acc.	Max Acc.	
ES	0.1	4.6	98.30%	0.48	4.85	76.86%	-	0.021	37.47%
FedAvg	4.2	73.7	98.09%	0.87	40.99	85.53%	0.266	2.134	50.22%
Fed-quant	1.7	41.8	98.15%	0.94	37.98	83.23%	0.086	0.800	49.78%
Fed-sparse	-	1.0	67.85%	2.78	17.13	73.17%	0.129	0.671	47.36%
EvoFed (our)	0.8	9.2	97.62%	0.75	7.78	84.72%	0.004	0.023	54.12%

Table 1: Performance of different schemes presented in tabular form, corresponding to Fig. 8.

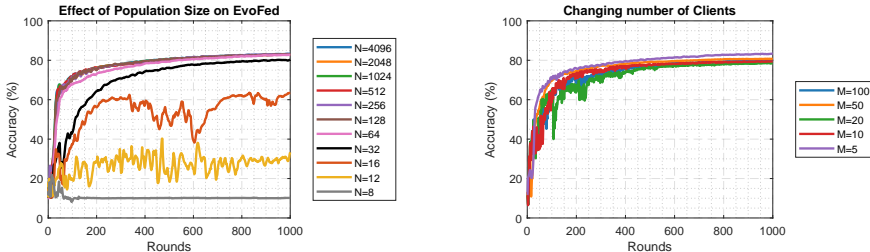
## 6 Results and Discussions

In this section, we discuss the experimental results in detail and provide further insights into the performance of EvoFed. The accuracy of EvoFed, compared with multiple baseline methods and different datasets, is shown in Fig. 8 (a), (b), and (c). Efficiently encoding and exchanging gradient information, EvoFed enhances the effectiveness of the ES algorithm across all tasks, delivering results comparable to FedAvg. Also, EvoFed achieves superior accuracy at an equivalent compression rate compared to sparsification. This suggests that utilizing a shared population of samples can reduce the information necessary for gradient compression, thereby enhancing the efficiency of the process. Fig. 8 (d), (e), and (f) shows the performance of each method as a function of communication load for all three datasets. It can be seen that EvoFed tends to utilize significantly less communication resources as compared to other high-accuracy techniques.

Table 1 summarizes the performance of different schemes on MNIST, FMNIST, and CIFAR-10 datasets, focusing on communication cost and accuracy. EvoFed achieves significantly lower communication costs compared to FedAvg while maintaining competitive accuracy levels. In the MNIST dataset, EvoFed achieves an accuracy of 97.62% with a mere 9.2 MB of communication load, while FedAvg achieves 98.09% accuracy at a considerably high communication cost of 73.7 MB. The effective compression achieved is an impressive 98.8% which indicates that the gradient vector is condensed into just 1.2% of the fitness vector that is communicated between clients and the server. Similarly, for the FMNIST dataset, EvoFed achieves an accuracy of 84.72% with only 7.78 MB of communication, whereas FedAvg’s accuracy is 85.53% with a communication cost of 40.99 MB. The efficiency of EvoFed becomes even more apparent in the CIFAR-10 dataset where the model compression is over 99.7%. EvoFed achieves an accuracy of 54.12% with a low communication cost of only 0.023 GB, surpassing FedAvg, which performs 50.22% at a communication cost of 2.134 GB. The simpler ES method actually gives better performance as well as higher communication efficiency than EvoFed for MNIST but its accuracy for other data sets is highly limited.

**Additional Experiments.** Fig. 9 illustrates the performance of EvoFed with varying numbers of samples  $N$  within the population and a varying number of clients  $M$ . The model’s performance is significantly influenced by the population size, which directly affects the algorithm’s exploration capability and compression rate. We observe a performance improvement as we increase the population size, although at the cost of increased computation and memory usage. Nonetheless, this improvement is not linear and plateaus once sufficient samples are generated to explore the parameter space. For instance, in the case of the FMNIST dataset and a model with 11K parameters, any performance enhancement beyond a generated sample size of 128 is marginal.

Fig. 9(b) showcases EvoFed’s performance trend as the number of clients increases. A minor performance decline is observable for some larger values of  $M$  relative to  $M=5$ . This decline could potentially be attributed to the limited data available per client and the increased variance associated with local training. Nonetheless, we believe that carefully tuning the hyperparameters based on data distribution could assist in achieving more robust performance.



(a) Varying number of population from 8 to 4096    (b) Varying number of clients from 5 to 100

Figure 9: Effect of population size (left) and number of clients (right) on EvoFed

Supplementary Materials provide further details regarding hyperparameters, model architectures, and experiments. We also include a detailed ablation study with different evolutionary strategies, the population size, and the number of partitions, as well as detailed communication and computational complexity analyses.

## 7 Conclusion

EvoFed, the novel paradigm presented herein, unites FL and ES to offer an efficient decentralized machine learning strategy. By exchanging compact fitness values instead of extensive model parameters, EvoFed significantly curtails communication costs. Its performance parallels FedAvg while demonstrating an impressive equivalent model compression of over 98.8% on FMNIST and 99.7% on CIFAR-10 in representative experimental settings. Consequently, EvoFed represents a substantial stride forward in FL, successfully tackling the critical issue of high communication overhead.

## Acknowledgments

A special acknowledgment goes to Do-yeon Kim for the valuable discussions on the convergence analysis presented in Section 4. This work was supported by the National Research Foundation of Korea (NRF) grant funded by the Korean government (MSIT) (No. NRF-2019R111A2A02061135), and by IITP funds from MSIT of Korea (No. 2020-0-00626).

## References

- [1] Jakub Konečný, H Brendan McMahan, Felix X Yu, Peter Richtárik, Ananda Theertha Suresh, and Dave Bacon. Federated learning: Strategies for improving communication efficiency. [arXiv preprint arXiv:1610.05492](#), 2016.
- [2] H Brendan McMahan, Eider Moore, Daniel Ramage, Seth Hampson, and Blaise Agüera y Arcas. Communication-efficient learning of deep networks from decentralized data. [arXiv preprint arXiv:1602.05629](#), 2016.
- [3] Jianyu Wang, Ananda Theertha Yu, and Gregory Wornell. Federated learning with matched averaging. [arXiv preprint arXiv:2002.06440](#), 2020.

- [4] Dan Alistarh, Demjan Grubic, Jerry Li, Ryota Tomioka, and Milan Vojnovic. Qsgd: Communication-efficient sgd via gradient quantization and encoding. In Advances in Neural Information Processing Systems, pages 1709–1720, 2017.
- [5] Yuzhu Mao, Zihao Zhao, Guangfeng Yan, Yang Liu, Tian Lan, Linqi Song, and Wenbo Ding. Communication-efficient federated learning with adaptive quantization. ACM Transactions on Intelligent Systems and Technology (TIST), 13(4):1–26, 2022.
- [6] Sebastian U Stich. Local sgd converges fast and communicates little. arXiv preprint arXiv:1805.09767, 2018.
- [7] Virginia Smith, Chao-Kai Chiang, Maziar Sanjabi, and Ameet S Talwalkar. Federated multi-task learning. In Advances in Neural Information Processing Systems, pages 4424–4434, 2017.
- [8] Felix Sattler, Simon Wiedemann, Klaus-Robert Müller, and Wojciech Samek. Robust and communication-efficient federated learning from non-iid data. In IEEE transactions on neural networks and learning systems, 2019.
- [9] Tian Li, Anit Kumar Sahu, Manzil Zaheer, Maziar Sanjabi, Ameet Talwalkar, and Virginia Smith. Fair resource allocation in federated learning. arXiv preprint arXiv:1905.10497, 2020.
- [10] Ronald J Williams. Simple statistical gradient-following algorithms for connectionist reinforcement learning. Reinforcement learning, pages 5–32, 1992.
- [11] Frank Sehnke, Christian Osendorfer, Thomas Rückstieß, Alex Graves, Jan Peters, and Jürgen Schmidhuber. Parameter-exploring policy gradients. Neural Networks, 23(4):551–559, 2010.
- [12] Daan Wierstra, Tom Schaul, Tobias Glasmachers, Yi Sun, Jan Peters, and Jürgen Schmidhuber. Natural evolution strategies. The Journal of Machine Learning Research, 15(1):949–980, 2014.
- [13] Xin Yao. Evolving artificial neural networks. Proceedings of the IEEE, 87(9):1423–1447, 1999.
- [14] Joel Lehman and Risto Miikkulainen. Neuroevolution. Scholarpedia, 8(6):30977, 2013.
- [15] Sebastian Risi and Julian Togelius. Neuroevolution in games: State of the art and open challenges. CoRR, abs/1410.7326, 2014.
- [16] Sebastian Risi and Julian Togelius. Neuroevolution in games: State of the art and open challenges. IEEE Transactions on Computational Intelligence and AI in Games, 9(1):25–41, 2015.
- [17] Daniel Golovin, John Karro, Greg Kochanski, Chansoo Lee, Xingyou Song, and Qiuyu Zhang. Gradientless descent: High-dimensional zeroth-order optimization. arXiv preprint arXiv:1911.06317, 2019.
- [18] Robert Tjarko Lange, Tom Schaul, Yutian Chen, Chris Lu, Tom Zahavy, Valentin Dalibard, and Sebastian Flennerhag. Discovering attention-based genetic algorithms via meta-black-box optimization. arXiv preprint arXiv:2304.03995, 2023.
- [19] Felix Sattler, Simon Wiedemann, Klaus-Robert Müller, and Wojciech Samek. Sparse binary compression: Towards distributed deep learning with minimal communication. In 2019 International Joint Conference on Neural Networks (IJCNN), pages 1–8. IEEE, 2019.
- [20] Jinjin Xu, Wenli Du, Yaochu Jin, Wangli He, and Ran Cheng. Ternary compression for communication-efficient federated learning. IEEE Transactions on Neural Networks and Learning Systems, 2020.
- [21] Eunjeong Jeong, Seungeun Oh, Hyesung Kim, Jihong Park, Mehdi Bennis, and Seong-Lyun Kim. Communication-efficient on-device machine learning: Federated distillation and augmentation under non-iid private data. arXiv preprint arXiv:1811.11479, 2018.
- [22] Sohei Itahara, Takayuki Nishio, Yusuke Koda, Masahiro Morikura, and Koji Yamamoto. Distillation-based semi-supervised federated learning for communication-efficient collaborative training with non-iid private data. arXiv preprint arXiv:2008.06180, 2020.

- [23] Felix Sattler, Arturo Marban, Roman Rischke, and Wojciech Samek. Communication-efficient federated distillation. arXiv preprint arXiv:2012.00632, 2020.
- [24] Tao Lin, Lingjing Kong, Sebastian U Stich, and Martin Jaggi. Ensemble distillation for robust model fusion in federated learning. Advances in Neural Information Processing Systems, 33: 2351–2363, 2020.
- [25] Chuhan Wu, Fangzhao Wu, Lingjuan Lyu, Yongfeng Huang, and Xing Xie. Communication-efficient federated learning via knowledge distillation. Nature communications, 13(1):1–8, 2022.
- [26] Mingzhe Chen, Nir Shlezinger, H Vincent Poor, Yonina C Eldar, and Shuguang Cui. Communication-efficient federated learning. Proceedings of the National Academy of Sciences, 118(17):e2024789118, 2021.
- [27] Takayuki Nishio and Ryo Yonetani. Client selection for federated learning with heterogeneous resources in mobile edge. In ICC 2019-2019 IEEE international conference on communications (ICC), pages 1–7. IEEE, 2019.
- [28] Canh T Dinh, Nguyen H Tran, Minh NH Nguyen, Choong Seon Hong, Wei Bao, Albert Y Zomaya, and Vincent Gramoli. Federated learning over wireless networks: Convergence analysis and resource allocation. IEEE/ACM Transactions on Networking, 29(1):398–409, 2020.
- [29] Alois Huning. Evolutionsstrategie. optimierung technischer systeme nach prinzipien der biologischen evolution, 1976.
- [30] Daan Wierstra, Tom Schaul, Jan Peters, and Jürgen Schmidhuber. Fitness expectation maximization. In Parallel Problem Solving from Nature–PPSN X: 10th International Conference, Dortmund, Germany, September 13-17, 2008. Proceedings 10, pages 337–346. Springer, 2008.
- [31] Sun Yi, Daan Wierstra, Tom Schaul, and Jürgen Schmidhuber. Stochastic search using the natural gradient. In Proceedings of the 26th Annual International Conference on Machine Learning, pages 1161–1168, 2009.
- [32] Yi Sun, Daan Wierstra, Tom Schaul, and Jürgen Schmidhuber. Efficient natural evolution strategies. In Proceedings of the 11th Annual conference on Genetic and evolutionary computation, pages 539–546, 2009.
- [33] Tobias Glasmachers, Tom Schaul, and Jürgen Schmidhuber. A natural evolution strategy for multi-objective optimization. In Parallel Problem Solving from Nature, PPSN XI: 11th International Conference, Kraków, Poland, September 11-15, 2010, Proceedings, Part I 11, pages 627–636. Springer, 2010.
- [34] Tobias Glasmachers, Tom Schaul, Sun Yi, Daan Wierstra, and Jürgen Schmidhuber. Exponential natural evolution strategies. In Proceedings of the 12th annual conference on Genetic and evolutionary computation, pages 393–400, 2010.
- [35] Tom Schaul, Tobias Glasmachers, and Jürgen Schmidhuber. High dimensions and heavy tails for natural evolution strategies. In Proceedings of the 13th annual conference on Genetic and evolutionary computation, pages 845–852, 2011.
- [36] Tim Salimans, Jonathan Ho, Xi Chen, Szymon Sidor, and Ilya Sutskever. Evolution strategies as a scalable alternative to reinforcement learning. arXiv preprint arXiv:1703.03864, 2017.
- [37] James C Spall. Multivariate stochastic approximation using a simultaneous perturbation gradient approximation. IEEE transactions on automatic control, 37(3):332–341, 1992.
- [38] Yurii Nesterov and Vladimir Spokoiny. Random gradient-free minimization of convex functions. Foundations of Computational Mathematics, 17:527–566, 2017.
- [39] W. Diffie and M. Hellman. New directions in cryptography. IEEE Transactions on Information Theory, 22(6):644–654, 1976. doi: 10.1109/TIT.1976.1055638.

- [40] Hangyu Zhu and Yaochu Jin. Real-time federated evolutionary neural architecture search. IEEE Transactions on Evolutionary Computation, 26(2):364–378, 2021.
- [41] Decebal Constantin Mocanu, Elena Mocanu, Peter Stone, Phuong H Nguyen, Madeleine Gibescu, and Antonio Liotta. Scalable training of artificial neural networks with adaptive sparse connectivity inspired by network science. Nature communications, 9(1):1–12, 2018.
- [42] Hangyu Zhu and Yaochu Jin. Multi-objective evolutionary federated learning. IEEE transactions on neural networks and learning systems, 31(4):1310–1322, 2019.
- [43] Zheng-yi Chai, Chuan-dong Yang, and Ya-lun Li. Communication efficiency optimization in federated learning based on multi-objective evolutionary algorithm. Evolutionary Intelligence, pages 1–12, 2022.
- [44] Qingfu Zhang and Hui Li. Moea/d: A multiobjective evolutionary algorithm based on decomposition. IEEE Transactions on evolutionary computation, 11(6):712–731, 2007.
- [45] Ivanoè De Falco, Antonio Della Cioppa, Tomas Koutny, Martin Ubl, Michal Krcma, Umberto Scafuri, and Ernesto Tarantino. A federated learning-inspired evolutionary algorithm: Application to glucose prediction. Sensors, 23(6):2957, 2023.
- [46] John Geweke. Antithetic acceleration of monte carlo integration in bayesian inference. Journal of Econometrics, 38(1-2):73–89, 1988.
- [47] Dimo Brockhoff, Anne Auger, Nikolaus Hansen, Dirk V Arnold, and Tim Hohm. Mirrored sampling and sequential selection for evolution strategies. In Parallel Problem Solving from Nature, PPSN XI: 11th International Conference, Kraków, Poland, September 11-15, 2010, Proceedings, Part I 11, pages 11–21. Springer, 2010.
- [48] Masahiro Yagisawa. Fully homomorphic encryption without bootstrapping. Cryptology ePrint Archive, 2015.
- [49] Hao Chen, Kim Laine, and Rachel Player. Simple encrypted arithmetic library-seal v2. 1. In Financial Cryptography and Data Security: FC 2017 International Workshops, WAHC, BITCOIN, VOTING, WTSC, and TA, Sliema, Malta, April 7, 2017, Revised Selected Papers 21, pages 3–18. Springer, 2017.
- [50] Junfeng Fan and Frederik Vercauteren. Somewhat practical fully homomorphic encryption. Cryptology ePrint Archive, 2012.
- [51] Ittai Anati, Shay Gueron, Simon Johnson, and Vincent Scarlata. Innovative technology for cpu based attestation and sealing. In Proceedings of the 2nd international workshop on hardware and architectural support for security and privacy, volume 13. ACM New York, NY, USA, 2013.
- [52] Han Xiao, Kashif Rasul, and Roland Vollgraf. Fashion-mnist: a novel image dataset for benchmarking machine learning algorithms. arXiv preprint arXiv:1708.07747, 2017.
- [53] Yann LeCun, Léon Bottou, Yoshua Bengio, and Patrick Haffner. Gradient-based learning applied to document recognition. Proceedings of the IEEE, 86(11):2278–2324, 1998.
- [54] Alex Krizhevsky and Geoff Hinton. Convolutional deep belief networks on cifar-10. Unpublished manuscript, 40(7):1–9, 2010.
- [55] James Bradbury, Roy Frostig, Peter Hawkins, Matthew James Johnson, Chris Leary, Dougal Maclaurin, George Necula, Adam Paszke, Jake VanderPlas, Skye Wanderman-Milne, and Qiao Zhang. JAX: composable transformations of Python+NumPy programs. Unpublished manuscript, 2018. URL <http://github.com/google/jax>.
- [56] Robert Tjarko Lange. evosax: Jax-based evolution strategies. arXiv preprint arXiv:2212.04180, 2022.

## Supplementary Materials

### A Complexity Analysis

Our proposed method significantly reduces communication overhead in federated learning. However, this reduction in communication comes at the cost of an increase in computation and memory usage on the client side. In this section, we provide a comprehensive analysis of these complexity trade-offs and discuss potential strategies to alleviate the added burdens. Specifically, we present an analysis of the computational, memory, and communication complexities of our proposed model and provide a comparative assessment against existing baselines.

In this analysis,  $E$  stands for the number of local epochs executed within a single communication round,  $M$  indicates the total number of clients,  $N$  represents the population size per client, and  $|\theta|$  denotes the dimension of the model parameter vector.

Table 2 presents the order of time and memory complexities for each method where we do not employ parallelization for ES and EvoFed computation. Here, clients generate perturbations one by one and reuse the memory after the fitness measurement of a perturbed sample. As shown in Table 2, EvoFed without parallelization has a similar order of memory complexity in clients to conventional FL, i.e., FedAvg, and reduced memory complexity in the server. However, in this scenario, the time complexity for EvoFed grows linearly with the number of perturbations as compared to FedAvg.

Table 2: Comparison of time and memory complexities for ES, EvoFed, and FedAvg, without parallel processing of  $N$  individual perturbed models.

Method	Client Time	Client Memory	Server Time	Server Memory
ES	$O(N \theta )$	$O( \theta )$	$O(N( \theta  + M))$	$O( \theta  + MN)$
EvoFed	$O(N \theta  + E \theta )$	$O( \theta )$	$O(N( \theta  + M))$	$O( \theta  + MN)$
FedAvg	$O(E \theta )$	$O( \theta )$	$O(M \theta )$	$O(M \theta )$

To mitigate the time complexity in EvoFed, one approach is to generate and evaluate a batch of  $T$  perturbations in parallel. This method poses a trade-off between time and memory complexity.

Partitioning (as discussed in the main text) is an alternative strategy that enables computing a higher number of fitness values for each perturbation by dividing it into  $K$  partitions. Consequently, the algorithm requires a fewer perturbations  $N'$  to obtain sufficient fitness values for gradient encoding, resulting in a reduction in memory complexity. This necessitates the transmission of  $N'K$  fitness values to the server. While partitioning does not introduce additional time complexity, having a small number of perturbations restricts the algorithm’s exploration capabilities in parameter space, as discussed in Section D.3. Therefore, in practice, we choose the population size to be  $\frac{N}{K} \leq N' \leq N$ , trading memory complexity with communication cost.

Table 3 provides a comparative analysis of the time and memory complexities for EvoFed and FedAvg when both  $T$  individual perturbed models are processed in parallel, and each perturbed model sample is divided into  $K$  partitions. In scenarios with enough memory, it is feasible to execute all perturbations in a parallel setting  $T = N$  and without partitioning  $K = 1$  and  $N = N'$ .

Table 3: Comparison of time and memory complexities for EvoFed and FedAvg, with parallel processing of  $T$  individual perturbed models and where each perturbation is partitioned to  $K$  segments.

Method	Client Time	Client Memory	Server Time	Server Memory
EvoFed (Parallel)	$O(\frac{N}{T} \theta  + E \theta )$	$O(T \theta )$	$O(\frac{N}{T}( \theta  + M))$	$O(N \theta  + MN)$
EvoFed (Partitioned)	$O(N' \theta  + E \theta )$	$O(N' \theta )$	$O(N'( \theta  + M))$	$O(N' \theta  + MKN')$
EvoFed (Both)	$O(\frac{N'}{T} \theta  + E \theta )$	$O(T \theta )$	$O(\frac{N'}{T}( \theta  + M))$	$O(N' \theta  + MKN')$
FedAvg	$O(E \theta )$	$O( \theta )$	$O(M \theta )$	$O(M \theta )$

As discussed before, the communication complexity of ES and EvoFed is limited to transferring fitness values  $O(N'K)$  while FedAvg is to the gradient signal  $O(|\theta|)$ . However we can apply additional compression on each method to reduce this complexity as explored in D.1 and D.2.

### B Model Architecture and Optimization Hyperparameters

We used a CNN model with 11k parameters for the MNIST and FMNIST datasets and a bigger model with 2.3M parameters for CIFAR-10, with architectural details provided in Table 6 and Table



7 respectively. We also provide detailed information about the optimization hyperparameters e.g. learning rate (lr), momentum and batch size, etc. for MNIST and FMNIST in Table 4 and for Cifar-10 in Table 5:

Table 4: Hyperparameters used in experiments on dataset MNIST & FMNIST

Model	Methods	Hyperparameters										
		batch size	lr	momentum	optimizer	$lr\_es$	$momentum\_es$	$optimizer\_es$	$w\_decay$	sigma	eps	$\beta\_1&\beta\_2$
CNN	ES	128	-	-	-	0.0148	0.9	sgd	0.0	0.27	1e-8	0.99 & 0.999
	FedAvg	256	0.0111	0.8099	sgd	-	-	-	-	-	-	-
	Fed-quant	256	0.0111	0.8099	sgd	-	-	-	-	-	-	-
	Fed-sparse	256	0.0111	0.8099	sgd	-	-	-	-	-	-	-
	<b>EvoFed (ours)</b>	256	0.0873	0.9074	sgd	0.0427	0.9	sgd	0.0152	0.27	1e-8	0.99 & 0.999

Table 5: Hyperparameters used in experiments on dataset CIFAR-10

Model	Methods	Hyperparameters										
		batch size	lr	momentum	optimizer	$lr\_es$	$momentum\_es$	$optimizer\_es$	$w\_decay$	sigma	eps	$\beta\_1&\beta\_2$
CNN	ES	32	-	-	-	0.04	0.4815	sgd	0.0	0.35	1e-8	0.99 & 0.999
	FedAvg	128	0.0009	0.6132	sgd	-	-	-	-	-	-	-
	Fed-quant	128	0.0009	0.6132	sgd	-	-	-	-	-	-	-
	Fed-sparse	128	0.0009	0.6132	sgd	-	-	-	-	-	-	-
	<b>EvoFed (ours)</b>	64	0.0148	0.3011	sgd	0.0275	0.5239	sgd	0.0824	0.35	1e-8	0.99 & 0.999

Table 6: Detailed information of the CNN architecture used in MNIST & FMNIST experiments

Layer	Parameter & Shape (cin, cout, kernal size) & hyper-parameters	#
layer1	conv1: $1 \times 8 \times 5 \times 5$ , stride:(1, 1); padding:0	$\times 1$
	avgpool	$\times 1$
layer2	conv1: $8 \times 16 \times 5 \times 5$ , stride:(1, 1); padding:0	$\times 1$
	avgpool	$\times 1$
	fc: $16 \times 10$	$\times 1$

Table 7: Detailed information of the CNN architecture used in CIFAR-10 experiments

Layer	Parameter & Shape (cin, cout, kernal size) & hyper-parameters	#
layer1	conv1: $3 \times 64 \times 5 \times 5$ , stride:(1, 1); padding:0	$\times 1$
	avgpool	$\times 1$
layer2	conv1: $64 \times 128 \times 5 \times 5$ , stride:(1, 1); padding:0	$\times 1$
	avgpool	$\times 1$
	fc: $128 \times 256$	$\times 1$
	fc: $256 \times 10$	$\times 1$

## C Convergence Analysis

**Assumption 1.** For each  $j$ ,  $L_j(v)$  is  $\beta$ -smooth, i.e.,  $\|\nabla L_j(u) - \nabla L_j(v)\| \leq \beta\|u - v\|$  for any  $u, v$ .

**Assumption 2.** Variance of the gradient of  $D_j$  is bounded,  $\mathbb{E} \left[ \left\| \nabla L_j(\theta) - \tilde{\nabla} L_j(\theta) \right\|^2 \right] \leq B^2$ .

**Assumption 3.** When perturbation  $\epsilon^i$  is sampled from the population distribution  $p_\psi$ , a conditioned mirrored sampling is applied such that  $\frac{1}{N} \sum_{i=1}^N \epsilon^i = 0$ ,  $\frac{1}{M} \sum_{i=1}^N (\epsilon^i)^2 \leq G^2$ ,  $\frac{1}{N} \sum_{i=1}^N (\epsilon^i)^3 = 0$ .

**Theorem 2.** Given a decreasing learning rate  $\eta_t < \frac{1}{4\alpha\beta}$ , EvoFed has the convergence bound as:

$$\frac{1}{H_T} \sum_{t=0}^{T-1} \eta_t \mathbb{E} \left[ \|\nabla L(\theta_t)\|^2 \right] \leq \frac{\mathbb{E} [L(\theta_0)] - L^*}{\alpha G^2 H_T} + 4\alpha\beta B^2 \left( \frac{1}{H_T} \sum_{t=0}^{T-1} \eta_t^2 \right)$$

where  $H_T = \sum_{t=0}^{T-1} \eta_t$ , and  $L^*$  represents the minimum value of  $L(\theta)$ .

By  $\beta$ -smoothness of  $L(\theta)$  and taking expectation on both sides, we have

$$\mathbb{E} [L(\theta_{t+1}) - L(\theta_t)] \leq \mathbb{E} [\langle \nabla L(\theta_t), \theta_{t+1} - \theta_t \rangle] + \frac{\beta}{2} \mathbb{E} [\|\theta_{t+1} - \theta_t\|^2] \quad (13)$$

**Proof.** By utilizing the proof of Lemma 1 and recognizing  $\langle \cdot, \cdot \rangle$  as the inner product operation, we rewrite the first term  $\mathbb{E} [\langle \nabla L(\theta_t), \theta_{t+1} - \theta_t \rangle]$  as follows:

$$\begin{aligned} \mathbb{E} [\langle \nabla L(\theta_t), \theta_{t+1} - \theta_t \rangle] &\stackrel{(a)}{=} \mathbb{E} \left[ \left\langle \nabla L(\theta_t), \frac{1}{M} \sum_{j=1}^M \frac{\alpha}{N\sigma} \sum_{i=1}^N f(\theta_{t,j} + \sigma \epsilon_t^i) \epsilon_t^i \right\rangle \right] \\ &\stackrel{(b)}{=} \mathbb{E} \left[ \left\langle \nabla L(\theta_t), \frac{1}{M} \sum_{j=1}^M \frac{\alpha}{N\sigma} \sum_{i=1}^N \left\| (\theta_{t,j} + \sigma \epsilon_t^i) - (\theta'_{t,j})^i \right\|^2 \epsilon_t^i \right\rangle \right] \\ &= -\mathbb{E} \left[ \left\langle \nabla L(\theta_t), \frac{1}{M} \sum_{j=1}^M \frac{\alpha}{N\sigma} \sum_{i=1}^N \left\| (\theta_{t,j} + \sigma \epsilon_t^i) \right. \right. \right. \\ &\quad \left. \left. \left. - (\theta_{t,j} - \eta_t \tilde{\nabla} L_j(\theta_{t,j})) \right\|^2 \epsilon_t^i \right\rangle \right] \\ &= -\mathbb{E} \left[ \left\langle \nabla L(\theta_t), \frac{1}{M} \sum_{j=1}^M \frac{\alpha}{N\sigma} \sum_{i=1}^N \left\| (\sigma \epsilon_t^i) + \eta_t \tilde{\nabla} L_j(\theta_{t,j}) \right\|^2 \epsilon_t^i \right\rangle \right] \\ &= -\mathbb{E} \left[ \left\langle \nabla L(\theta_t), \frac{1}{M} \sum_{j=1}^M \frac{\alpha}{N\sigma} \sum_{i=1}^N \left( \sigma^2 (\epsilon_t^i)^3 + 2\sigma (\epsilon_t^i)^2 \eta_t \tilde{\nabla} L_j(\theta_t) \right. \right. \right. \\ &\quad \left. \left. \left. + \epsilon_t^i \eta_t^2 \|\tilde{\nabla} L_j(\theta_t)\|^2 \right) \right\rangle \right] \\ &\stackrel{(c)}{\leq} -\mathbb{E} \left[ \left\langle \nabla L(\theta_t), \frac{1}{M} \sum_{i=j}^M \frac{\alpha}{\sigma} \left( 2\sigma G^2 \eta_t \tilde{\nabla} L_j(\theta_t) \right) \right\rangle \right] \\ &\stackrel{(d)}{=} (-2\alpha\eta_t G^2) \mathbb{E} \left[ \left\langle \nabla L(\theta_t), \frac{1}{M} \sum_{j=1}^M \nabla L_j(\theta_t) \right\rangle \right] \\ &\stackrel{(e)}{=} (-\alpha\eta_t G^2) \left\{ \mathbb{E} [\|\nabla L(\theta_t)\|^2] + \mathbb{E} \left[ \left\| \frac{1}{M} \sum_{j=1}^M \nabla L_j(\theta_t) \right\|^2 \right] \right. \\ &\quad \left. - \underbrace{\mathbb{E} \left[ \left\| \nabla L(\theta_t) - \frac{1}{M} \sum_{j=1}^M \nabla L_j(\theta_t) \right\|^2 \right]}_{=0} \right\} \end{aligned}$$

where (a) comes from the Lemma 1, (b) is due to  $f(\theta_t) = -\|\theta_t - \theta'_t\|^2$ , (c) follows from Assumption 3, (d) is from taking expectation for the mini-batch, and (e) is due to the well-known equality  $\|z_1 - z_2\|^2 = \|z_1\|^2 + \|z_2\|^2 - 2\langle z_1, z_2 \rangle$ .

On the other hand, we can bound the second term  $\mathbb{E} [\|\theta_{t+1} - \theta_t\|^2]$  as follows:

$$\begin{aligned}
\mathbb{E} [\|\theta_{t+1} - \theta_t\|^2] &= \mathbb{E} \left[ \left\| \frac{1}{M} \sum_{j=1}^M \frac{\alpha}{N\sigma} \sum_{i=1}^N f(\theta_t + \sigma \epsilon_t^i) \epsilon_t^i \right\|^2 \right] \\
&= \mathbb{E} \left[ \left\| \frac{1}{M} \sum_{j=1}^M \frac{\alpha}{N\sigma} \sum_{i=1}^N \|(\theta_t + \sigma \epsilon_t^i) - \theta'_t\|^2 \epsilon_t^i \right\|^2 \right] \\
&= \mathbb{E} \left[ \left\| \frac{1}{M} \sum_{j=1}^M \frac{\alpha}{N\sigma} \sum_{i=1}^N \|(\theta_t + \sigma \epsilon_t^i) - (\theta_t - \eta_t \tilde{\nabla} L_j(\theta_t))\|^2 \epsilon_t^i \right\|^2 \right] \\
&= \mathbb{E} \left[ \left\| \frac{1}{M} \sum_{j=1}^M \frac{\alpha}{N\sigma} \sum_{i=1}^N \left( \sigma^2 (\epsilon_t^i)^3 + 2\sigma (\epsilon_t^i)^2 \eta_t \tilde{\nabla} L_j(\theta_t) + \epsilon_t^i \eta_t^2 \|\tilde{\nabla} L_j(\theta_t)\|^2 \right) \right\|^2 \right] \\
&\stackrel{(a)}{\leq} \mathbb{E} \left[ \left\| \frac{1}{M} \sum_{j=1}^M \frac{\alpha}{\sigma} \left( 2\sigma G^2 \eta_t \tilde{\nabla} L_j(\theta_t) \right) \right\|^2 \right] = \mathbb{E} \left[ (4\alpha^2 G^2 \eta_t^2) \left\| \frac{1}{M} \sum_{j=1}^M \tilde{\nabla} L_j(\theta_t) \right\|^2 \right] \\
&\stackrel{(b)}{\leq} (8\alpha^2 G^2 \eta_t^2) \mathbb{E} \left[ \left\| \frac{1}{M} \sum_{j=1}^M \nabla L_j(\theta_t) \right\|^2 + \left\| \frac{1}{M} \sum_{j=1}^M \nabla L_j(\theta_t) - \frac{1}{M} \sum_{j=1}^M \tilde{\nabla} L_j(\theta_t) \right\|^2 \right] \\
&\stackrel{(c)}{\leq} (8\alpha^2 G^2 \eta_t^2) \left\{ \mathbb{E} \left[ \left\| \frac{1}{M} \sum_{j=1}^M \nabla L_j(\theta_t) \right\|^2 \right] + B^2 \right\}
\end{aligned}$$

where (a) comes from Assumption 3, (b) is due to  $\|a + b\|^2 \leq 2\|a\|^2 + 2\|b\|^2$ , and (c) is by Assumption 2.

By applying the aforementioned bounds of  $\mathbb{E} [\langle \nabla L(\theta_t), \theta_{t+1} - \theta_t \rangle]$  and  $\mathbb{E} [\|\theta_{t+1} - \theta_t\|^2]$  to (13), we obtain:

$$\begin{aligned}
\mathbb{E} [L(\theta_{t+1}) - L(\theta_t)] &\leq \mathbb{E} [\langle \nabla L(\theta_t), \theta_{t+1} - \theta_t \rangle] + \frac{\beta}{2} \mathbb{E} [\|\theta_{t+1} - \theta_t\|^2] \\
&\leq \mathbb{E} \left[ (-\alpha \eta_t G^2) \left\{ \|\nabla L(\theta_t)\|^2 + \left\| \frac{1}{M} \sum_{j=1}^M \nabla L_j(\theta_t) \right\|^2 \right\} \right. \\
&\quad \left. + (4\alpha^2 \beta G^2 \eta_t^2) \left\{ \left\| \frac{1}{M} \sum_{j=1}^M \nabla L_j(\theta_t) \right\|^2 + B^2 \right\} \right] \\
&= -\alpha \eta_t G^2 \mathbb{E} [\|\nabla L(\theta_t)\|^2] \\
&\quad + \underbrace{\alpha \eta_t G^2 (4\alpha \beta \eta_t - 1) \mathbb{E} \left[ \left\| \frac{1}{M} \sum_{j=1}^M \nabla L_j(\theta_t) \right\|^2 \right]}_{\leq 0 \text{ if we choose } \eta_t \leq \frac{1}{4\alpha\beta}} + (4\alpha^2 \beta G^2 \eta_t^2) B^2 \\
&\leq -\alpha \eta_t G^2 \mathbb{E} [\|\nabla L(\theta_t)\|^2] + (4\alpha^2 \beta G^2 \eta_t^2) B^2
\end{aligned}$$

Eventually, through the telescoping sum for  $t = 0, 1, \dots, T - 1$ , we obtain

$$L^* - \mathbb{E}[L(\theta_0)] \leq \sum_{t=0}^{T-1} (-\alpha\eta_t G^2) \mathbb{E}[\|\nabla L(\theta_t)\|^2] + \sum_{t=0}^{T-1} (4\alpha^2\beta G^2 \eta_t^2) B^2$$

where  $L^*$  represents the minimum value of  $L(\theta)$ .

After performing division on both sides by  $H_T = \sum_{t=0}^{T-1} \eta_t$ , and employing some manipulations, we obtain

$$\frac{1}{H_T} \sum_{t=0}^{T-1} \eta_t \mathbb{E}[\|\nabla L(\theta_t)\|^2] \leq \frac{\mathbb{E}[L(\theta_0)] - L^*}{\alpha G^2 H_T} + 4\alpha\beta B^2 \left( \frac{1}{H_T} \sum_{t=0}^{T-1} \eta_t^2 \right) \quad (14)$$

By utilizing a decreasing learning rate (e.g.,  $\eta_t = \frac{\eta_0}{1+t}$ ), it can be seen that  $H_T = \sum_{t=0}^{T-1} \eta_t \rightarrow \infty$  as  $T$  increases, while  $\sum_{t=0}^{T-1} \eta_t^2 < \infty$ . Consequently, the upper bound stated in Equation (14) approaches 0 as  $T$  grows, ensuring convergence towards a stationary point.

## D Additional Experimental Result

In this section, we delve into the impacts of various parameters on both the training and communication rate. We first study the role of population size and the number of clients. Subsequently, we investigate the effect of additional compression techniques, such as sparsification, ranking, and quantization, on the model’s performance. Lastly, we assess the efficacy of partitioning on clients in attaining better accuracy, and its relationship with the population size.

### D.1 Fitness Vector Sparsification (Top-k Subset Selection)

In this section, we explore the effect of fitness sparsification i.e. selecting top-k fitness values from the fitness vector of the whole population based on magnitude. We examined the effects of sparsification on two distinct population sizes: 128 and 1024. Without any sparsification, both populations demonstrated comparable performance. However, when we select the top-k most fit values, the denser population (comprising 1024 members) could tolerate a higher degree of sparsification compared to the less populous one (with 128 members).

To enable a fair and insightful comparison between the two population sizes, our focus was on assessing performance based on the number of members remaining post-sparsification rather than directly contrasting sparsification rates. We placed particular emphasis on the best and worst performing members, as they exert the most significant influence on the model update process in ES.

Fig. 10(a) and (b) visualize the sparsification process for populations of 128 and 1024, respectively, illustrating the performance decline that occurs as the number of remaining members diminishes.

Fig. 10(c) provides further insights into the performance improvements achieved by selecting top-8 or top-16 members from the initial set of 128 or 1024, as compared to optimizing with the whole population of 8 or 16.

Our results underline the crucial role that population size plays in exploring optimal solutions, overshadowing even the significance of compression rate. A larger population allows for broad exploration that can later be compressed to a smaller number of members without a performance loss. However, initiating the process with a smaller population cannot achieve equivalent performance due to the restricted exploration. Therefore, population size is a critical factor affecting the efficacy of exploration in evolutionary strategies.

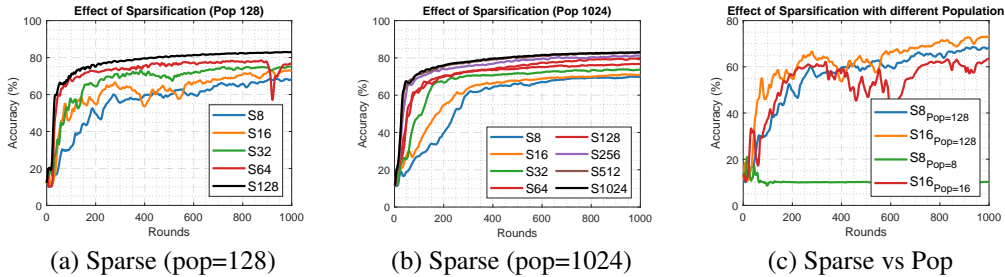


Figure 10: Effect of sparsification on EvoFed

## D.2 Ranking and Quantization

In this section, we examine the sensitivity of EvoFed to the precise value of fitness. We propose two techniques to reduce the bits required to represent the fitness vector, thus enhancing compression without compromising performance. For a clearer understanding of these methods’ impacts, we chose a population size of 32, which is relatively less populated and has minimal redundancy, highlighting the insensitivity of EvoFed to precise fitness values.

Fig. 11(a) depicts the effect of quantization with varying bit numbers. The legend represents the number of bits used for quantization as a numeral followed by the letter  $Q$ , where  $Q32$  indicates no compression and  $Q1$  signifies transmitting a single bit (either 0 or 1) in place of the fitness value. The result exhibits a marginal performance loss even with  $Q2$ , illustrating EvoFed’s insensitivity to precise fitness values and the potential for further compression gains through quantization.

Fig. 11(b) presents the performance when we transmit the member’s rank within the population instead of the fitness value. In the legend, the number of samples assigned the same rank is denoted as a numeral following the letter  $R$ ;  $R32$  indicates assigning 32 different ranks to all members, and  $R1$  implies assigning the same rank to every member. This ranking technique, a common practice in the Evolutionary Strategies literature, is typically employed when fitness values derived from the environment are noisy, and the quality of the solution can be improved by transmitting the ranking instead. However, where we have high-quality fitness measures derived from L2 loss, this technique only slightly improves the performance while reducing compression gains. By assigning the same rank to neighbouring samples within the fitness ranking, we can further enhance compression performance.

Comparing ranking and quantization, it is observed that quantization delivers superior performance with the same number of bits. Additionally, the number of bits used in quantization is independent of the population size, making quantization a more appropriate approach for compressing fitness values.

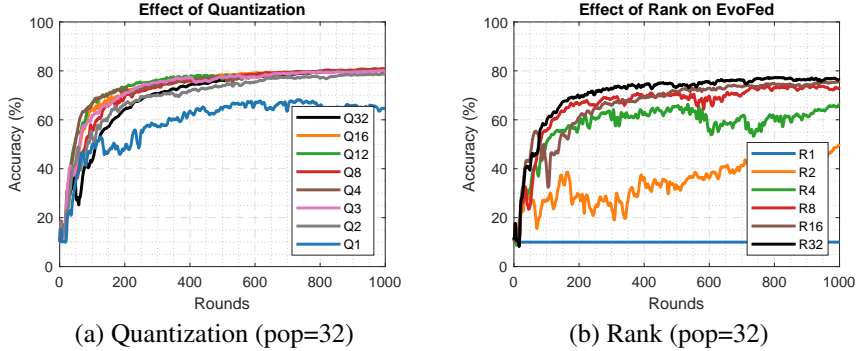


Figure 11: Effect of Quantization on EvoFed

## D.3 Partitioning

The EvoFed’s partitioning technique, as described in the main text, features a unique attribute that enhances performance. This technique maintains a fixed number of population samples at each client, thereby addressing memory limitations on the clients but necessitating increased communication as a trade-off. Although sparsification results underscore the importance of population size for exploration, partitioning presents an additional approach that navigates the limitation posed by the compression rate to improve performance.

Fig. 12 illustrates the impact of partitioning in four scenarios, each with a different population size. The results emphasize that partitioning is most effective when the clients cannot manage a sufficient number of samples to attain satisfactory performance. Partitioning enables us to gather more information from the limited sample size.

Each sub-figure in Fig. 12 includes baselines without partitioning, allowing for the comparison of improvements achievable either through an increased population size or the use of more partitions while maintaining a consistent communication rate. The legend of each figure specifies the number of partitions (the number following the letter  $k$ ) and the population of the baselines (the number following the letter  $p$ ). The volume of information required to be communicated for one round is also depicted for each method in the legend.

Fig. 12 clearly shows that using population sizes of 32 and 128 results in only a marginal improvement in performance. However, when utilizing population sizes of 8 and 16, a significant and noticeable improvement can be observed.

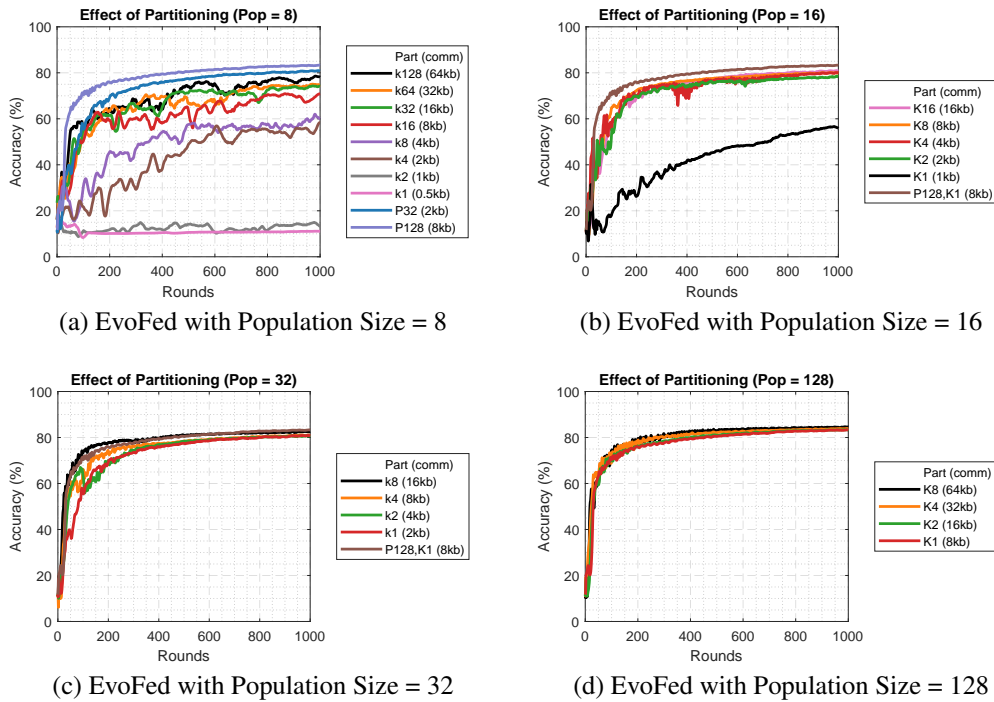


Figure 12: Effect of partitioning on EvoFed

#### D.4 Larger Dataset and Model

Additionally, we investigate the efficacy of EvoFed in the context of a larger model and a bigger dataset. Fig. 13(a) showcases the performance on CIFAR-100 dataset with the same model parameters as those used in the CIFAR-10 experiment. The results show that EvoFed, although having a slower convergence rate, achieves higher performance than FedAvg eventually, with a significant compression rate. Fig. 13(b) illustrates the performance gain on CIFAR-10 dataset when the CNN layers are doubled. As the experimental result shows, having a larger model generally leads to better performance with slower convergence. EvoFed follows the same trend as BP in a centralized setting, suggesting the compression has not been affected by model size. All experiments were conducted with a population size of 32 and 50 partitions.

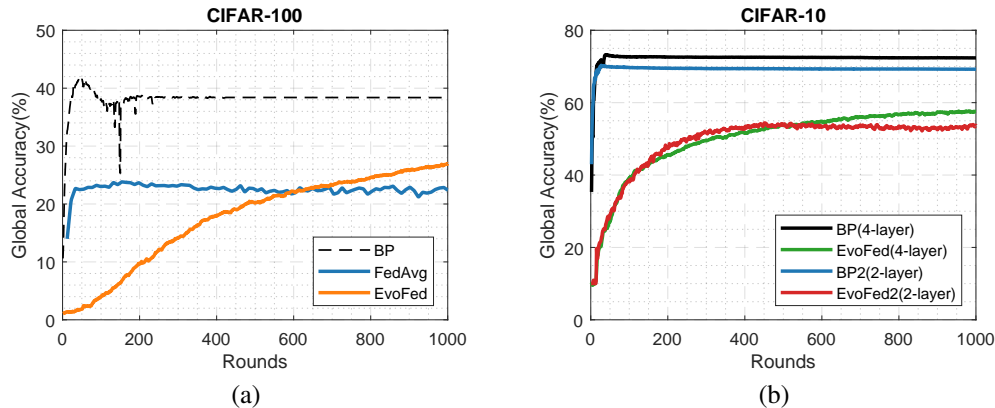


Figure 13: Larger dataset and Model: (a) shows performance on CIFAR-100, and (b) depicts the impact of having a larger model on CIFAR-10.